Pollution Scavenging by Rain Falling Through a Polluted Low-Level Air Layer

by

P. B. Storebø

and

A. N. Dingle

FOREWORD

The present report is the product of research done by the authors during the sabbatical leave of Professor Dingle from his teaching duties during the winter term, January to May, 1972. The hospitality of Dr. Storebø and his colleagues at the Norwegian Defense Research Establishment, Kjeller, was most gracious, and their society both pleasant and stimulating. The result of the collaboration, here reported, has numerous ramifications in connection with air pollution, rain chemistry, haze and fog formation, and the generation of cloud and rain.

ABSTRACT

The vapor and heat transfer equations are used sequentially in a stepwise computational procedure which models heterogeneous nucleation and growth of haze and fog upon pollution particles. The procedure requires a numerical feed-back technique which links the heat and vapor transfer processes and enables an account of droplet temperatures and liquid water contents, by size category, to be maintained throughout the computations. An important result is that maximum cloud air supersaturations of two per cent and more are indicated even for slowly cooling air, although the supersaturations with respect to the droplet surfaces are limited to a few tenths of a per cent as indicated by previous work. The model assumes mixed nuclei composed of ammonium sulfate and graphite, and it includes removal of the pollution and fog water by an overriding steady rain.

I. INTRODUCTION

The increasing occurrence of soiled snow and acid rain over the last two decades (Granat, 1972) has become a matter of public concern, not free of alarm, in Norway. The dramatic decrease of the fish population in the lakes of southern Norway, and the reportedly sharp reduction of forest growth rates in the same area both impact heavily upon key resources of the Norwegian economy. Although the conditions producing these effects are not at present fully understood, it is widely inferred that a major contributor is airborne sulfur, and sulfates, the principal source of which is the industrial and population centers of Europe, notably the Ruhr, the Rhine and the Meuse Valleys, and to a lesser extent the industrial centers of Great Britain.

The synoptic weather situation typical of the most highly polluted cases is characterized by an anticyclone over eastern to central Europe and a cyclonic system approaching the continent from the west. These systems together produce a strong southerly flow at low level, confined under the frontal and subsidence inversions, and a steady light rain generated above the warm-frontal inversion ahead of the (usually) occluded front. Thus the heavy pollution load is carried primarily at low level and tends to be "washed out" by the overriding rain without strong participation in the rain-generating processes. This scavenging situation has been

described indirectly by Bergeron (1960) who has named the upper cloud deck the "seeder" and the lower level fog and/or stratus the "feeder" in his studies of Scandinavian precipitation patterns.

In the present work a computational model of this set of circumstances is presented. As the polluted air flows inland, it is raised orographically to a maximum elevation of 300 m over a distance of 20 km. The path continues at constant elevation for 10 km and then descends steadily to 150 m above sea level 10 km farther inland. The computations follow the air elements along the path giving the complete history of the growth of the pollution particles by condensation. The droplet temperatures, hygroscopicities, and the rates of removal by the superimposed steady rain are also computed for each particle size class throughout the path length. The influences of such parameters as initial temperature, humidity, rainfall rate, and wind speed are explored.

2. THE AIR POLLUTION PARTICLES

The model pollution particles are chemically mixed, each containing a chemically active and an inactive component. Because of widespread current interest in ammonium sulfate, we have chosen this to be the active component. The density and specific heat of graphite are used for the inactive component.

The particle size spectrum is constructed by first specifying the total mass of each component per cm^3, and by distributing this mass according to a log-normal distribution. For the inactive component the basic data specify 4×10^{-11} gm per cm^3 distributed around a modal radius of 10^{-5} cm with a standard deviation of 2.5; for the active component the corresponding statistics are 10^{-11} gm per cm^3, 5×10^{-6}cm, and 2.5,respectively.

After computing the size distributions for the active and inactive components separately, the masses are combined class-by-class to give a "mixed nucleus" size spectrum. Thirty size classes are used,the smallest having an initial radius of 1.5×10^{-6} cm, and the class size interval being chosen to double the volume of the particles from one size class to the next, i.e., $d(\ln r) = 1/3 \ln 2$. The largest particle class thus has an initial radius of 1.33×10^{-3} cm.

The effects of the electrolytic solute upon the formation of fog in the pollution cloud are computed by means of the formulation of Low (1969a) in which the mean ionic activity coefficients, $\gamma_{\pm}$, the solute activity, a', and the water activity, a, are used to express the departures of the electrolytic solutions from ideality. The water activity, a, is defined by

$$a = p/p_0 \tag{2.1}$$

where p and p_0 are the equilibrium vapor pressures over plane surfaces of solution and pure water, respectively. The molal activity of the electrolyte, a', is given by

$$a' = (\nu_+^{\nu_+} \cdot \nu_-^{\nu_-}) m^{\nu} \gamma_{\pm}^{\nu} \tag{2.2}$$

where ν_+ is the number of moles of cations per mole of electrolyte

ν_- is the number of moles of anions per mole of electrolyte

$\nu = \nu_+ + \nu_-$

and m is the molality of the solution.

The Gibbs-Duhem equation gives the relation of a to a':

$$n \, d(\ln a) + n' \, d(\ln a') = 0 \tag{2.3}$$

where n is the number of moles of solvent, and n' is that of

the solute. Low shows that $\underline{a}$ is related to the practical osmotic coefficient, ϕ, by

$$a = \exp(-\nu w m \phi) \tag{2.4}$$

where $w = \frac{M}{1000}$, M = molecular wt. of water. Finally, the Kelvin curvature effect is invoked to give the equilibrium vapor pressure with respect to a solution droplet of radius $\underline{r}$:

$$p = p_0 a \exp(2M\sigma'/\rho' RTr) \tag{2.5}$$

where σ' and ρ' are respectively the surface energy and the density of the solution at temperature T. Inasmuch as Low presents tabulations of $\underline{a}$ against molality, $\underline{m}$, equation (2.5) is most convenient for use in the computations. This tabulation is limited in the case of ammonium sulfate to a maximum molality of 5.5, corresponding closely to saturation of the solution at 25C. The activity coefficient varies by less than 1 percent from 25C to 0C, and by less than 0.1 percent from 1013.25 to 500 mb (Harned and Owen, 1958), so we must have assumed that Low's table is accurate enough for the immediate purpose. In addition although it is clear that the molality of the saturated solution depends upon temperature, we have neglected this effect. The water activity $\underline{a}$ thus varies from a minimum of 0.8124 to 1.000 in the computations.

The effects of temperature and molality upon σ' are assumed to be independent and to follow the formula

$$\sigma'(T,m) = \sigma(T,0) + \Delta\sigma(m) \qquad (2.6)$$

where $\sigma(T,0)$ expresses the temperature dependence of pure water surface energy, and $\Delta\sigma(m)$ expresses the incremental contribution of the solute as a function of molality at 25C. The value of $\sigma(T,0)$ is approximated by the following four points between which linear interpolation is used:

t °C =	+20	0	-7	-13
(T,0) =	72.8	75.6	76.75	78.5

The incremental effect of the dissolved material is approximated from Low's (1969b) curve by

$$\Delta\sigma = 2.18m \qquad (2.7)$$

The solution density, ρ', is derived from a table (Hodgeman, 1961) which is stored in the computer memory, using molality as the independent variable. Linear interpolation is used between the tabulated values during the computations. The thermal effect upon ρ', within the context of the present work is small. Inasmuch as it behaves badly near the freezing point, and is dependent both upon temperature and molality, we have chosen to neglect it. Suitable consideration of this factor should probably enter a more refined future model.

3. TEMPERATURE AND VAPOR ACCOUNTS

The low level air is assumed to remain at constant temperature and pressure until it is elevated orographically. Cooling is then initiated by adiabatic expansion in an atmosphere the pressure profile of which is determined hydrostatically. In this part of the computations the assumption is made that the gradient of virtual temperature experienced in the most recent time step may be used to compute the new pressure.

The initial adiabatic temperature change leads to phase changes of the airborne water substance. In each time step, condensation upon the droplets (nuclei) of each particle size class is treated without reference to the other classes. As water is acquired, the particle mass and radius are increased accordingly, then the solution molality and equilibrium vapour density are computed. At each step the temperature for each particle-size class is recomputed taking into account the release of latent heat, the effect of adiabatic cooling and the heat transfer to the air environment of the particles. The influence among the size classes comes about through the vapor concentration and air temperature which are reset according to the totals of condensation and heat transfer before a new time step is taken.

The heat of condensation is considered to be supplied directly to the pollution droplets, warming them in the condensation stages and cooling them during evaporation. The effect upon air temperature is then computed using the conductive transfer equation (4.4). The results show that deviations of the droplet temperatures from the air temperature are generally small and nearly constant from one time step to the next. Thus the heat of condensation is supplied to or provided by the air itself in accord with the wet adiabatic assumption.

The air temperature is also affected by the conversion of kinetic energy from the droplets and the raindrops to heat:

$$\Delta Q = \sum_i n_i v_i m_i g \Delta t$$

where n_i is the number of drops or droplets in size class i, v_i is their terminal fall speed, m_i is their mass, and g is the gravitational acceleration.

The accounting procedure is based upon unit mass of pure dry air because the number of pollution particles associated with this unit is conservative with respect to volume changes and phase changes of water. The mixing ratio therefore is the parameter used for water vapor accounting. After each time step the vapor condensed on all the pollution droplets in unit mass of pure dry air is subtracted from the mixing ratio to give the value for the next time step.

The raindrops, which continuously fall through the air elements under study, also affect the temperature and the vapor budgets through phase changes and heat transfer. A correct treatment of these effects requires that the thermal history of the raindrops be known. This is beyond the scope of the present model. Rather, it is assumed that the raindrops have the temperature of the air, and that their equilibrium vapor concentration corresponds to saturation over pure water.

4. CONDENSATION AND EVAPORATION OF WATER

A solution droplet of radius r changes in size by vapor diffusion as long as the vapor concentration c of the environment differs from that for equilibrium over the droplet surface, c_{eq}. Maxwell's (1927) expression for mass rate of growth under quasistatic conditions is modified by Fuchs (1959) and Squires (1952) to give

$$\frac{dm}{dt} = 4\pi r D (c - c_{eq}) \beta_m V \qquad (4.1)$$

where D is the diffusion coefficient for water vapor in air, β_m, is the Fuchs correction factor for condensation on small drops, V is the Squires ventilation factor, and c_{eq} is the vapor pressure leading to no mass change for the droplet. D is tabulated (Hodgeman, 1961) and a linear formula for

the temperature dependence is used for D measured in $cm^2.s^{-1}$.

$$D = 0.2264 + 0,001394(T_a - 273.16) \qquad (4.2)$$

where T_a is the air temperature.
For β_m Fuchs' expression is used without modification. The value of V is computed using the following formula

$$V = 2480 \cdot r^2 = 38.8 \cdot r + 1.024$$

which is derived from Squires' table of ventilation factors. In the computation, an absolute limit arbitrarily set to 2 is placed upon V.

The vapor concentration values, c and c_{eq}, together determine whether condensation or evaporation will occur. In general

$$c = \frac{pM}{RT} \qquad (4.3)$$

in which p is the relevant vapor pressure, i.e., the ambient environmental vapor pressure on the one hand, and the equilibrium vapor pressure over the droplet surface on the other. The latter is given by equation (2.5). It is clear that

the influence of the droplet temperature in determining c_{eq} is dominant. Computation and use of the droplet temperature, T_p, is thus a vital part of the computations.

The temperature increase of the droplet by conduction from its environment is given by

$$C \cdot \frac{dTp}{dt} = 4\pi rK(T_a - T_p)\beta_T V$$

$$= A(T_a - T_p) \qquad (4.4)$$

where C is the droplet heat capacity

T_a the environmental air temperature

β_T the Fuchs correction factor for heat transfer

V the Squires ventilation factor

and K is the heat conduction coefficient for air given by

$$K = 2395 + 81038\ (T_a - 273.16) \qquad (4.5)$$

The development of condensation is followed in short time steps, Δt, during the computations. The mass of water condensed and the amount of heat transferred are computed separately in sequence. Since in nature these processes are obviously simultaneous and strongly interconnected, a numerical feed-back technique is used in the computations. The reasoning follows.

If all latent heat released during a time step in the condensation process is supplied to the droplet at the

beginning of the time interval, the course of the temperature required by (4.4) will be

$$T_p = T_p' e^{-At/C} + T_a\left(1 - e^{-At/C}\right) \qquad (4.6)$$

where T_p' is the initial droplet temperature. The mean temperature for the time interval Δt is therefore

$$\overline{T_p} = \frac{C}{A \cdot \Delta t}\left(T_p' - T_a\right)\left(1 - e^{-A\Delta t/C}\right) + T_a \qquad (4.7)$$

Because the heat loss is directly proportional to the product $(T_a - T_p)dt$, a droplet with constant temperature $\overline{T_p}$ over the whole time interval must experience the same heat loss as one following the temperature course of (4.6). $\overline{T_p}$ then, is the temperature that the droplet would assume if the condensation heat were evenly supplied throughout $\underline{\Delta t}$, and is further the temperature for which the equilibrium vapor concentration should be computed. A satisfactory treatment also requires knowledge about the rate of temperature change with mass condensed.

If the droplet temperature before warming by condensation heat is T_0, it is possible to define the ratio of the mean temperature rise to the initial temperature rise obtained from the stepwise computation:

$$\frac{\overline{T_p} - T_0}{T_p' - T_0} = \mu \gtrsim 1 - e^{-A\Delta t/C} \frac{C}{A\,t} \qquad (4.8)$$
$$\lesssim 1$$

Knowledge of μ should enable the numerical integration of (4.1). To explore further, consider that the condensation of a mass m of vapor leads to a temperature increase of the droplet which is approximately

$$\Delta\overline{T_p} = \Delta T_p \cdot \mu = \frac{m\left[L + C_w(T_a - T_p)\right]}{C} \cdot \mu \qquad (4.9)$$

The corresponding equilibrium vapor concentration is

$$c_{eq} = c_{eq}' + \frac{dc_{eq}}{dT_p} \cdot \Delta\overline{T_p} \qquad (4.10)$$

The temperature dependence of c_{eq} upon $\overline{T_p}$ is given by the saturation vapor pressure equation of Goff and Gratch (1946). For the present computations it is assumed that dc_{eq}/dT_p may be adequately approximated by the local tangent to the Goff-Gratch curve, and (4.9) and (4.10) are combined to give

$$c_{eq} = c_{eq}' + \left(\frac{dc_{eq}}{dT}\right)_{Tp'} \cdot \frac{m \cdot \left[L + C_w(T_a - T_p)\right]}{C} \cdot \mu$$
$$= c_{eq}' + \alpha \cdot m \qquad (4.11)$$

The value of c_{eq} corresponding to $\overline{T_p}$ is given by (4.11) as long as the value of m and the effects of the condensation upon c_{eq} are correctly judged. Small deviations from the

estimate are automatically corrected for by the heat and vapor accounting procedures.

Introducing (4.11) into (4.1), we write

$$\frac{dm}{dt} = B(c - c_{eq}' - \alpha \cdot m)$$

which may be solved for m corresponding to the time interval Δt, giving

$$m = \frac{c - c_{eq}'}{\alpha}\left(1 - e^{-\alpha B \Delta t}\right) \qquad (4.12)$$

To apply the outlined procedure, it is necessary that the ratio, μ, be approximately constant. Results of the computations show that μ varies by less than 0.001 of its value per time step, increasing smoothly with droplet size. As a result, a high degree of accuracy is obtained by using the value of μ from the preceding time step for each size class. The growth of the smallest droplets is shown by this procedure to be mainly determined by the vapor diffusion rates whereas heat conduction becomes the controlling factor for the largest droplets.

5. THE RAINDROP-SIZE SPECTRUM AND POLLUTION REMOVAL

The model includes rainfall from an independent higher-altitude cloud deck. The general assumption is made

that impact-collection of the pollution droplets by the falling raindrops is the only means of removing them from the air. By means of the formulation of Marshall and Palmer (1948)

$$N_i = N_o \cdot \exp(-41.0 \cdot P^{-0.21 D_i}) \cdot dD$$

where

D_i is the raindrop diameter in cm

P is the rate of rainfall in $mm \cdot h^{-1}$

N_i is the number of raindrops per unit volume in a class i with diameter width dD,

the raindrop number in each drop-size class is computed. The raindrop-size distribution is limited to 17 size classes at 0.2 mm intervals to a maximum of 3.4 mm diameter.

The fall speed, V_i, of the raindrops is computed using the formulation of Dingle and Lee (1972)

$$V_i = -17.8951 + 448.9498D + 16.3719D^2 - 45.9516D^3; \quad D \leq 1.4 \text{ mm}$$

and

$$V_i = 24.1660 + 448.8336D - 15.6265D^2 + 4.2695D^3, \quad D > 1.4 \text{ mm}$$

The removal of the pollution droplets by the raindrop population is based on collision efficiency values

adapted from Mason (1971). These are composite results assembled from a number of different authors.

Although Mason's contribution in assembling this table is greatly appreciated, there is difficulty in using it as presented. A few apparent editorial errors are readily detected and corrected, but in addition certain domains of oscillatory fluctuation appear. These suggest the influence of computational inaccuracy rather than physical variation.

The present procedure requires interpolation between tabulated values. It is felt that the physical situation calls for smooth variation of the collision efficiencies across the drop and droplet spectra. Smoothing has therefore been applied to the Mason values, and the computational table has been read from the resulting curves shown in Figure 5.1. For droplets smaller than 2 μm radius, zero efficiency has been used. The upper-limit of 20 μm was never exceeded. It is recognized that this treatment is an interim solution, useful only for the immediate purpose at hand.

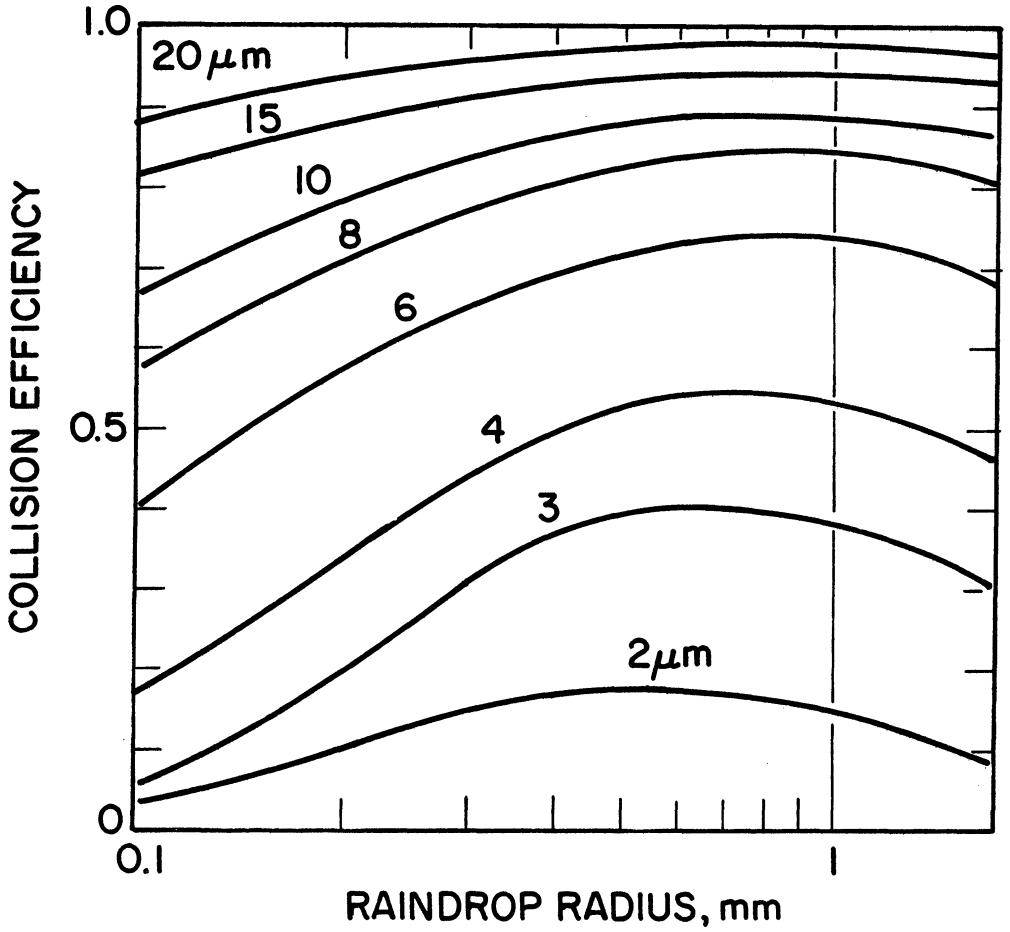

Figure 5.1 Collision efficiencies for raindrops, $0.1 \leq r \leq 1.7$ mm, upon cloud droplets, $2 \leq r \leq 20$ μm, adapted from Mason (1971).

6. INITIAL CONDITIONS AND PRELIMINARY ADJUSTMENT

The modeled cases are specified in terms of arbitrarily selected initial conditions defined by temperature, humidity, pressure, wind, rainfall intensity and pollution load. The initial barometric pressure was always set at 1013.25 mb. Values specified for the other variables are listed in Table 6.1.

Table 6.1 Conditions for the Modeled Cases

Initial Values				Wind Speed	Rainfall Intensity
		Pollution Load gm cm^{-3}			
Temp. °K	Rel. Humid. %	Active	Inactive	m/sec^{-1}	mm hr^{-1}
268	90	10^{-12}	4×10^{-12}	2	2
278	100	2.5×10^{-12}	10^{-11}	5	5
293	110	5×10^{-12} 10^{-11}	2×10^{-11} 4×10^{-11}	10	10

The values joined by the dashed line are those which we identify as the "baseline case". The effect of varying each of these quantities is examined by holding all other conditions to the baseline values as the variable under study assumes its other values.

At the stated relative humidities, the model pollution particles should normally have acquired water from the

vapor. To model the approach of the airborne particles toward equilibrium with air of the humidities specified, an adjustment period of 100 time steps is allowed prior to beginning the model air trajectory. In this period (400 sec in most cases), all of the particles acquire some water and the relative humidity is correspondingly reduced. The adjusted initial state thus achieved is a non-equilibrium state of slow vapor flux from the smallest toward the largest droplets.

7. GENERAL ASPECTS OF PHASE CHANGES AND SCAVENGING

An overall view of the results of the baseline computation is given in Figures 7.1 and 7.2. The path profile is given at the bottom of each figure. The air moves over this path as a 5 m sec^{-1} breeze, thus the vertical rise rate during the first 4000 sec (0 to 20 km) is 7.5 cm sec^{-1}, and the descent rate during the last 2000 sec is the same.

The most conspicuous feature of the condensation course is a maximum in relative humidity about 3 km from the origin. A similar feature has been noted earlier by other authors treating condensation (Howell, 1949; Mordy, 1959; Neiburger and Chien, 1960). The obvious reason is that the total condensation capability is low when the bulk of the droplets is small. The liquid water amount increases by a factor of two hundred up to the peak relative humidity reflecting the rapid growth of the droplets during this period. Once the maximum is passed, indicating that the condensation rate has surpassed

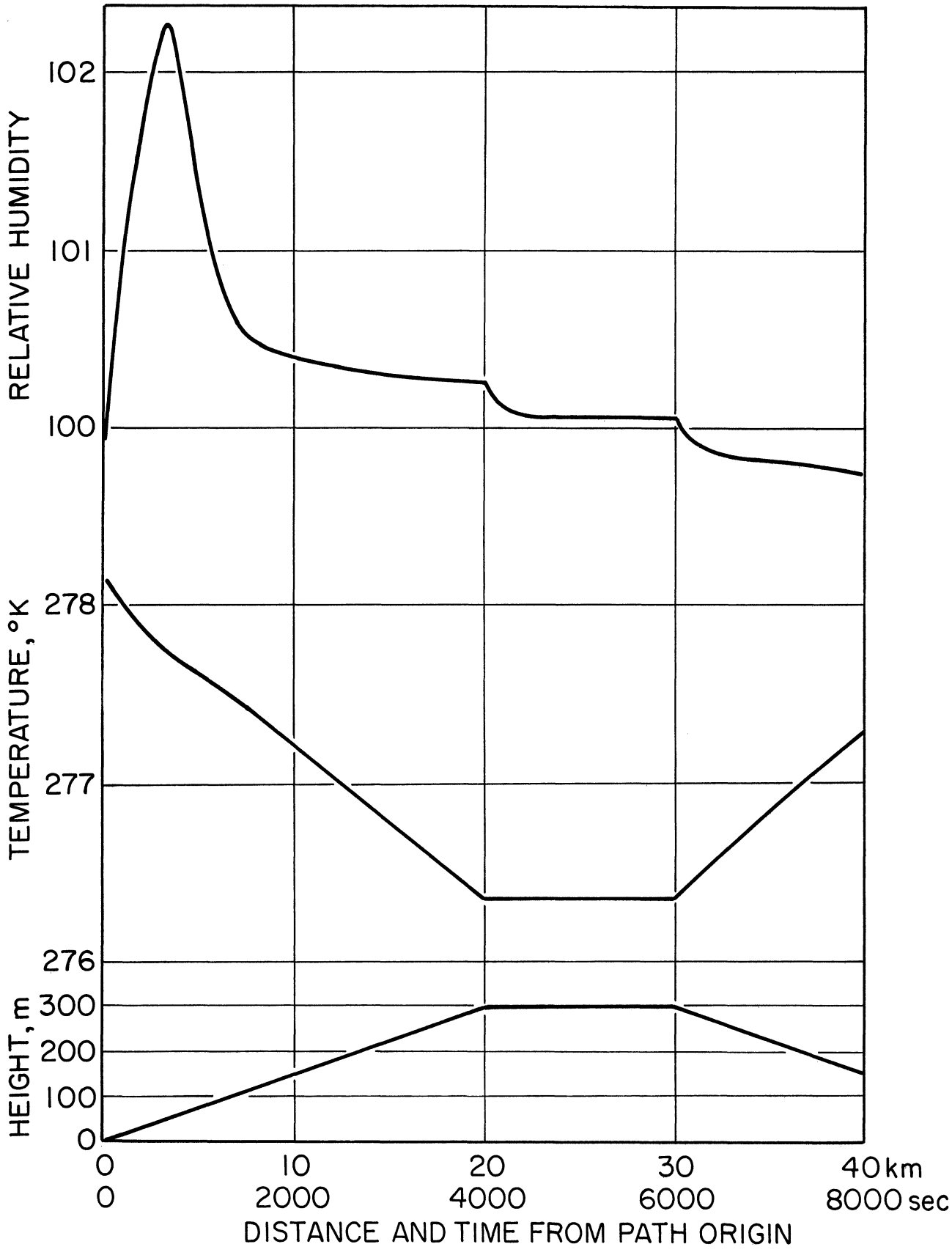

Figure 7.1 Course of relative humidity and temperature along the path, baseline case.

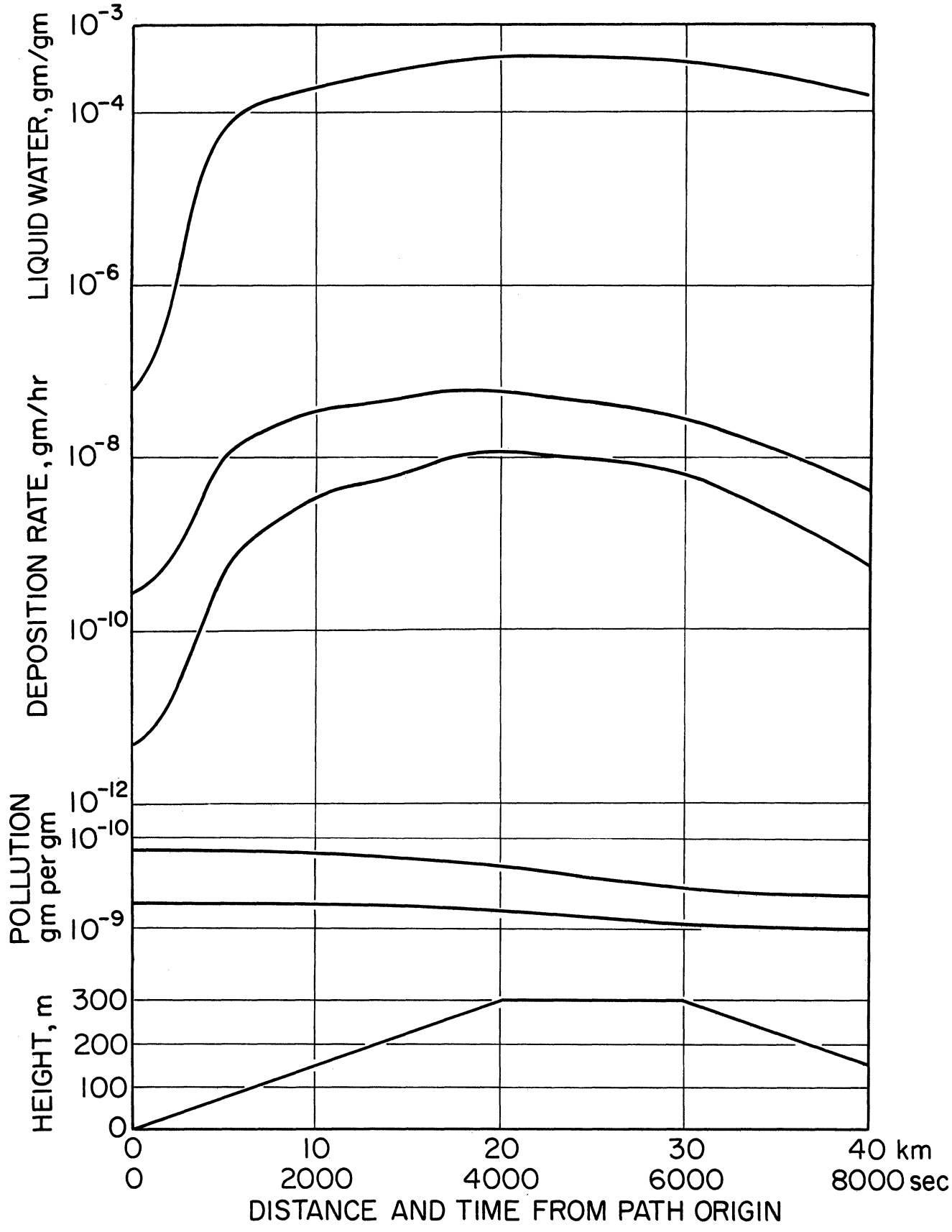

Figure 7.2 Course of liquid water and pollution deposition rate along the path, baseline case.

equality with the vapor supply, the relative humidity falls off to a pseudo-steady state, which is disturbed whenever the rate of ascent is changed.

As long as the droplet distribution cannot consume the vapor supply, the air temperature approximately follows the dry adiabatic rate. Afterwards the course follows the moist adiabatic rate, and in a transition period during the most intense condensation, the earlier temperature deficit is compensated. Similar small adjustments also occur where the path profile shows a bend, leading to a shift in the relative humidity level. The temperature during descent is slightly higher than during ascent in response to droplet scavenging in combination with a delay in the response to phase changes of water.

The liquid water content increases throughout the period of upslope motion, achieving a maximum at the edge of the plateau. The reduction beyond this point is attributed to scavenging of the droplets by the scavenging rain; the mass of pollution particles decreases along the path for the same reason. The rate of removal is low when the droplets are small but increases rapidly after the relative humidity peak is passed and the droplets grow large enough to be scavenged efficiently. The maximum scavenging rate occurs just at the edge of the plateau.

A difference in the scavenging rate for the active and inactive pollution components giving mass reductions of

30 and 50 per cent, respectively, are noted. This reflects the difference between the modes of the two size distributions and is therefore expected.

The development of the droplet size distribution is shown in Figure 7.3. First it is seen that during the "adjustment" period, all the pollution particles acquire water, and the greatest growth is found in size classes 6 to 10 ($.0476 \leq r_p \leq .1276\mu m$). The radial growth rate maximum shifts to smaller sizes as the air is lifted. When the edge of the plateau is reached, the growth pattern shifts because of cessation of lifting, and the smallest droplets are seen to evaporate as the larger droplets continue to grow, but slowly. The evaporation process is accentuated during the descent, and at the end of the path, the largest droplets are just beginning to lose water.

The course of the droplet temperatures is shown in Figure 7.4. During the lifting-condensation period, all the drops maintain temperatures above that of the air, and the warmest droplets are the largest ones. The greatest temperature excess overall and in each class is observed at the peak of relative humidity. At this point the high temperature of the drops exerts a strong brake upon the condensation rate because it effectively reduces the air-to-droplet vapor gradient. The variation of the temperature excess across the size spectrum tends to suppress condensation more upon the large drops than upon the small ones. This effect is most marked during

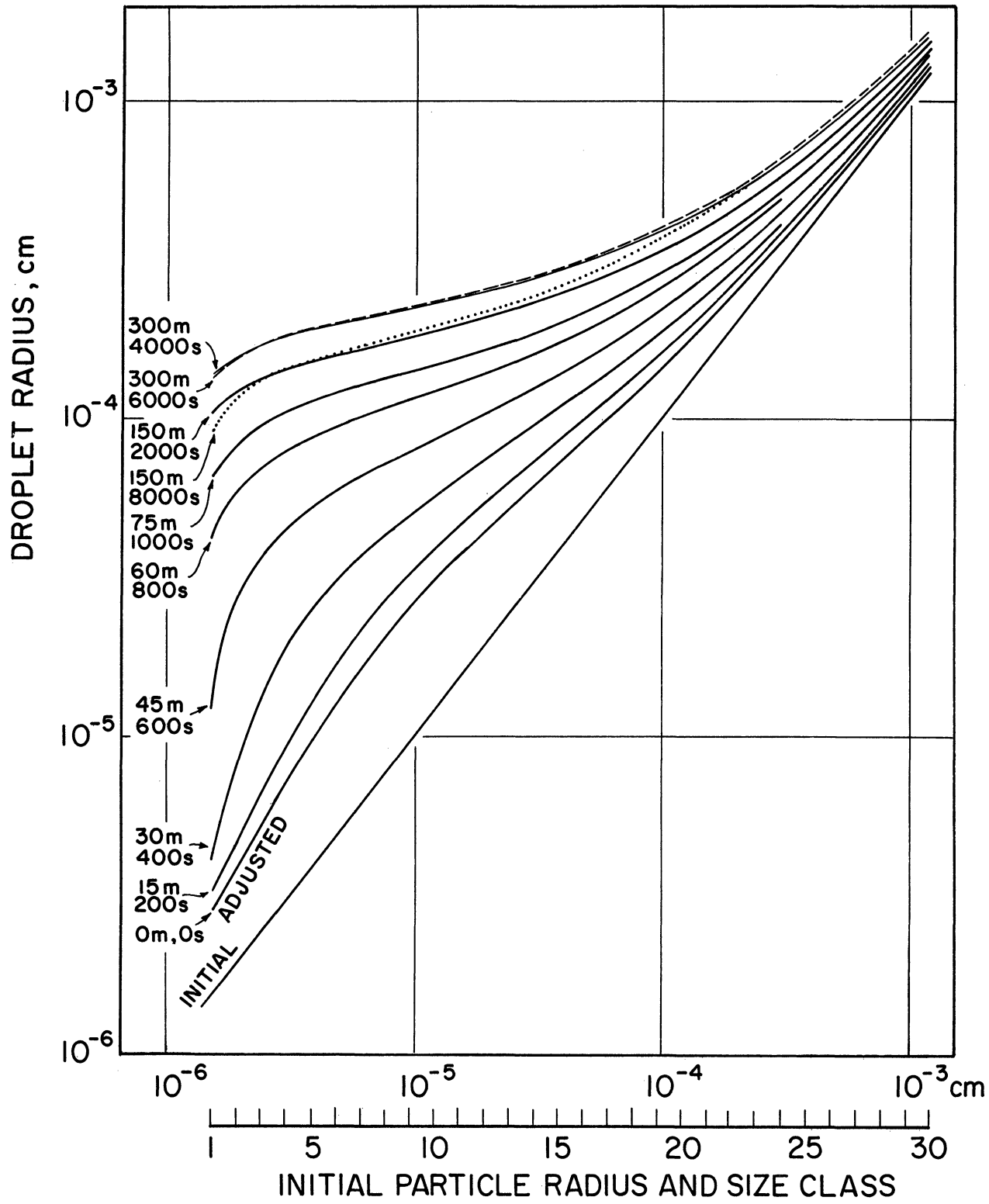

Figure 7.3 Development of the droplet size distribution. The solid curves show the particle/droplet sizes at the times and heights indicated. The dashed curve shows the status at the far edge of the plateau (at 6000 sec, 300 m); the dotted curve shows that after the descent to 150 m (8000 sec).

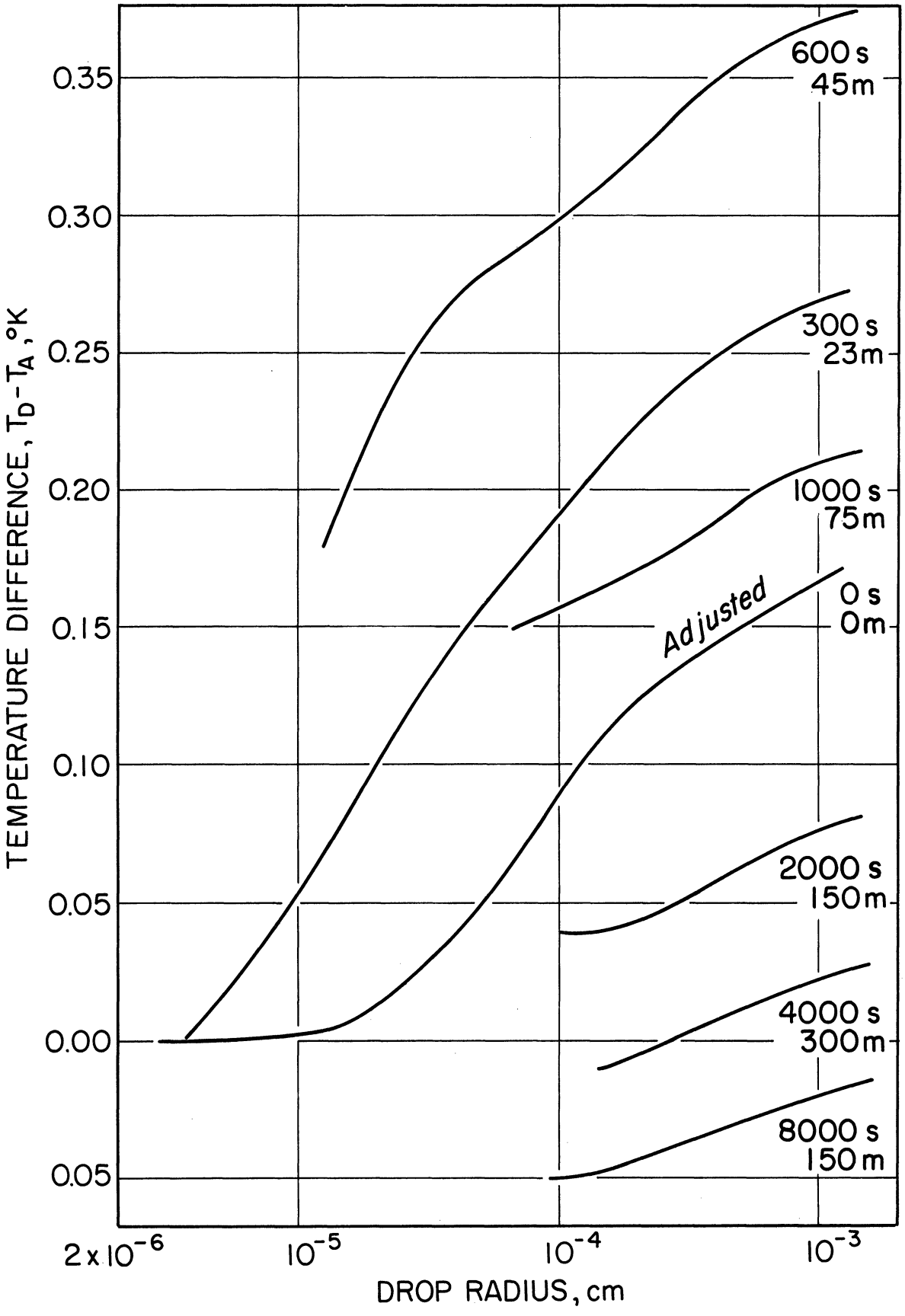

Figure 7.4 Deviation of droplet temperature from air temperature. Labels give time in sec and elevation in m from path origin.

the period of highest relative humidity. This temperature effect is therefore an important factor which tends to produce a compressed droplet size distribution when the rate of condensation is rapid.

As condensation proceeds, the slope of the curve becomes smaller and quasi-constant, and the temperature excess decreases. On the plateau (4,000 to 6,000 sec) the smallest droplets are colder than the environment, a consequence of evaporation during adjustment of the droplet distribution. For the chosen path the same temperature gradient appears also at 8000 sec where evaporation has taken place and all droplets are colder than the air. The largest droplets have just started to evaporate, and the picture is not necessarily typical for more vigorous evaporation over the whole distribution.

The equilibrium humidity for the droplets is always close to the atmospheric humidity level. The droplet temperature, size and content of soluble electrolyte all affect the droplet equilibrium humidity value (equation 2.5). The ratio of this value to the saturation humidity corresponding to the air temperature can be compared to the relative humidity of the cloud air.

Development of the humidity with respect to the droplet distribution is shown in Figure 7.5. The relative humidity is higher than the equilibrium requirement for the

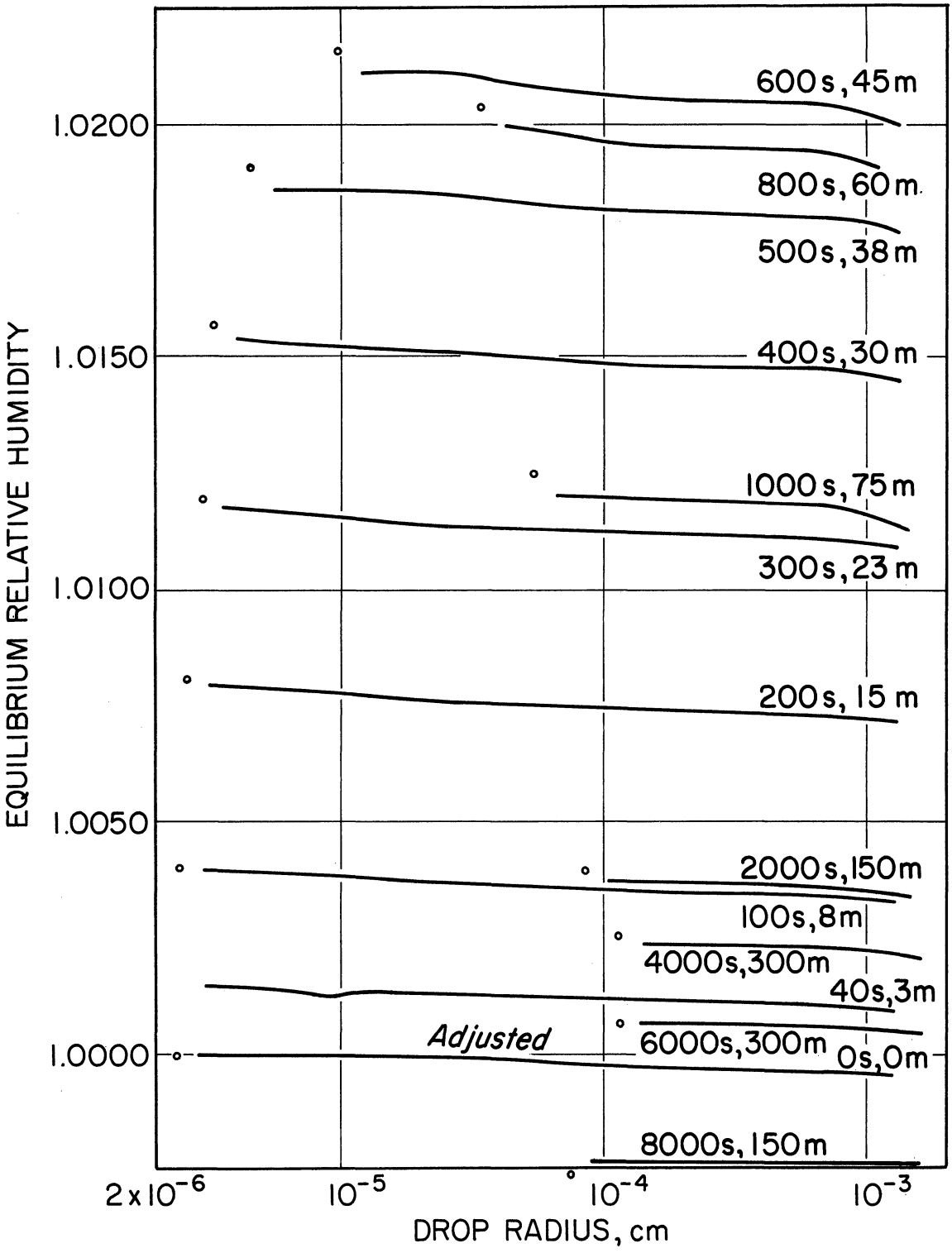

Figure 7.5 Ratio of droplet equilibrium humidity to saturation humidity at air temperature, and relative humidity of the cloud air. The latter is the ratio of the water vapor mixing ratio to the saturation mixing ratio, and thus gives the result of the total condensation/evaporation for each time step. It is shown by the plotted point for each path position. Labels give time and elevation from path origin.

whole droplet distribution during ascent, and the difference is greatest when the relative humidity has its peak. This is also the moment when greatest variation is found within the distribution itself. In spite of the relative warmness of the largest drops, their equilibrium humidity values are consistently below those for the smaller, cooler drops. This trend is persistent throughout the course of the computations.

Along the plateau (the 6000 sec curve) the relative humidity requirement is not fulfilled for droplets smaller than 1.5μm radius, which consequently evaporate, while condensation takes place for most of the others. The plateau in the model is only 10 km long, and is traversed in slightly more than half an hour. During this time the relative humidity is gradually lowered, and the boundary between evaporation and condensation slowly shifts toward larger droplet sizes. The shift is much more rapid during the descent. At 7000 sec droplets smaller than 10 μm radius evaporate, while at 8000 sec all droplets have undergone some evaporation.

The scavenging effect is shown in Figure 7.6. Scavenging is not effective in the smallest size classes because the collision efficiencies are assumed to be zero for all droplets smaller than 2 μm in radius. In contrast, the number of the largest particles is reduced by a factor of 10^6 over the whole path. As long as the droplets are growing, increasingly smaller particles are affected by scavenging.

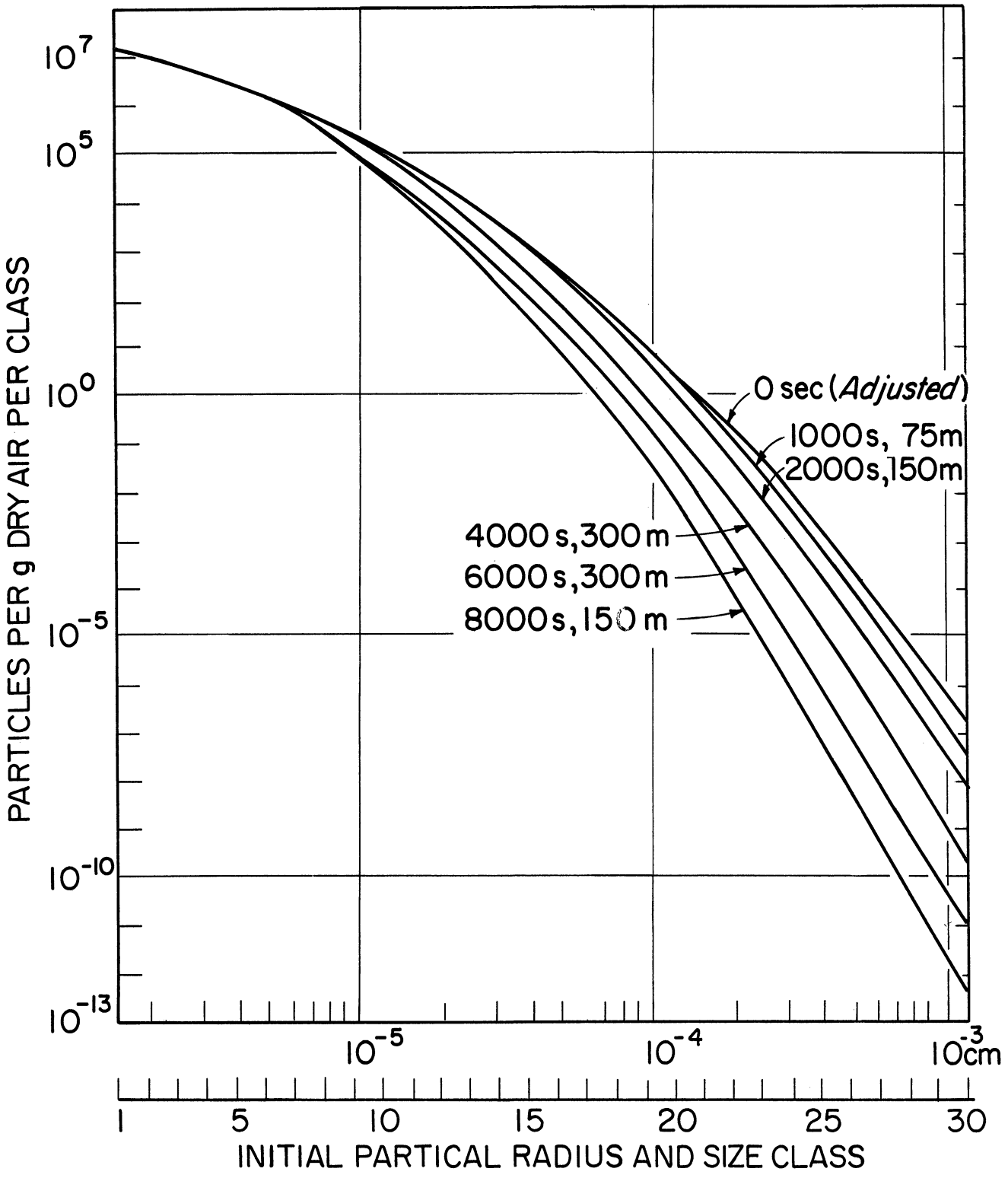

Figure 7.6 Number of particles per gm of dry air as a function of initial size and time for initial pollution load of 2.5×10^{-11} gm cm^{-3}. Labels give time and elevation from path origin.

8. RESPONSES TO INDIVIDUAL PARAMETER CHANGES

As indicated above (section 6), variations from the baseline case were studied by varying one parameter at a time from its baseline values. The cases studied are indicated above. Possible changes that were not studied include variations of the particle modes and size distributions, relative shifts in the distributions of active and inactive masses, changes of the active ingredient, and variations of the path.

8.1 AMOUNT OF POLLUTION

Within the context of the present model, the amount of airborne pollution affects only the number of particles.

The developing peak in relative humidity soon after the start of ascent increases slightly with decreasing particle number. However, the further course is not much affected. The available water is obviously divided among the particles present, and the result is bigger droplets. The droplet size distribution at the top of the ascent is shown in Figure 8.1 for various numbers of particles with the same internal distribution. In addition to being larger, the droplets tend to become more nearly equal in size with decreasing number. This may be an effect of the higher relative humidity during condensation.

As shown by Figure 8.2, the bigger droplets lead to more rapid scavenging of both pollution and liquid water.

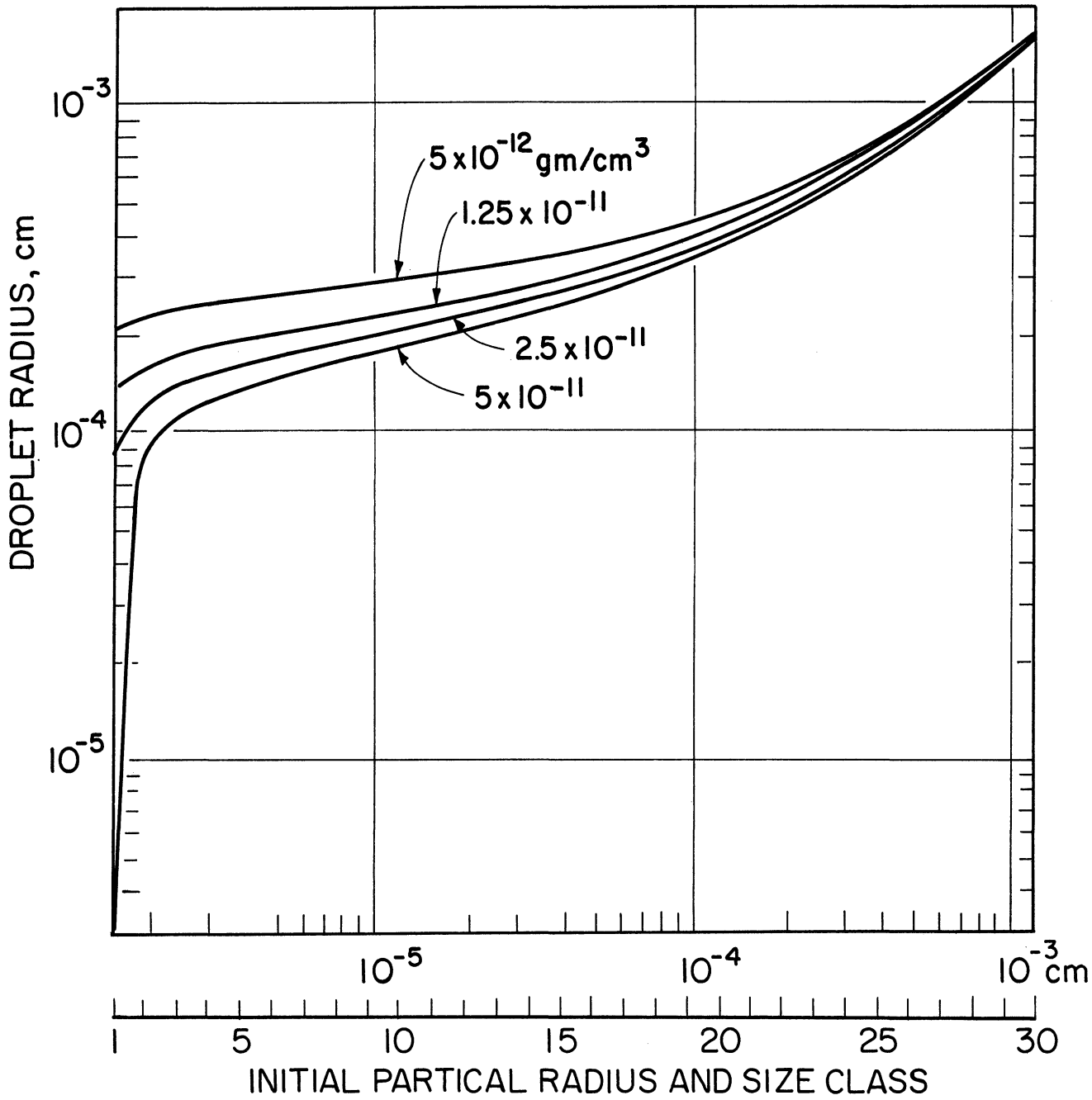

Figure 8.1 Droplet sizes at the top of the ascent (4000 sec) for different initial pollution concentrations. Total initial pollution amounts are noted in gm cm^{-3}.

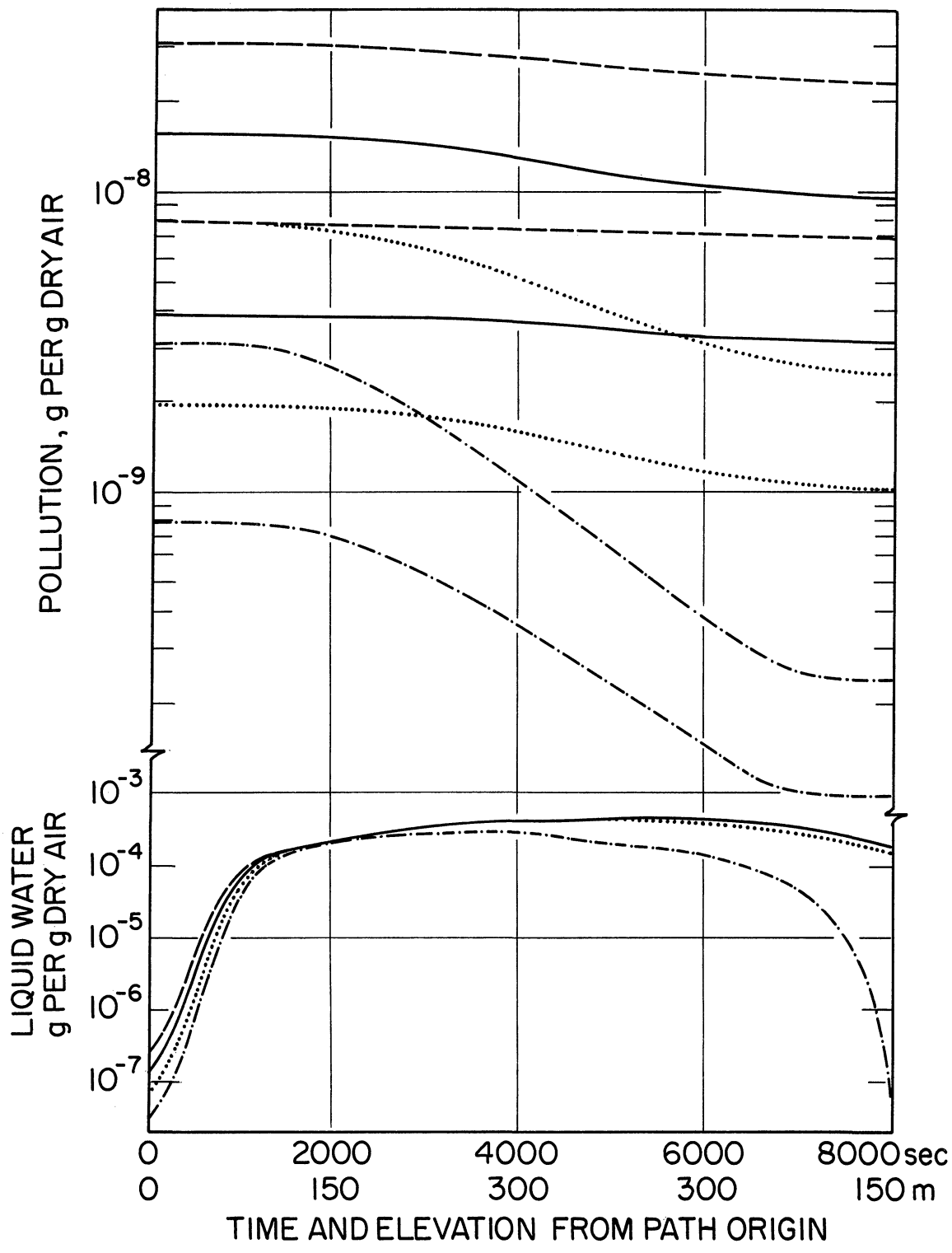

Figure 8.2 Course of pollution amounts and development of liquid water concentrations along the path. Pollution amounts are shown as active (lower) and inactive components for total initial masses of 2.5×10^{-11} (solid line), 5×10^{-11} (dashed), 1.25×10^{-11} (dotted), and 0.5×10^{-11} (dash-dot) gm cm^{-3}. Liquid water curves correspond to these respective cases.

8.2 WIND SPEED

Wind speed has two basic effects. The first of these is that it, together with the orography of the specified path, determines the rate of change of the variables of state. The second is that it determines the length of time required for the pollution cloud to traverse the path, hence the amount of modeled rain that falls through and scavenges polluted droplets.

Figure 8.3 shows how relative humidity, liquid water content, and pollution amount change along the path at three different wind speeds. With increasing wind speed (equivalent to increasing ascent rate) the initial relative humidity maximum increases and occurs farther up the slope. With respect to time, the peak occurs earlier as the wind speed increases (Table 8.1). This behavior is a consequence of

Table 8.1 Relative Humidity Maximum, Position and Time vs Wind Speed

Wind Speed m/sec	Ascent Rate cm/sec	Relative Humidity Maximum			
		Value %	Position		Time sec.
			HT,m.	Distance,km	
2	3.0	101.26	30.0	2	1000
5	7.5	102.30	50.6	3.38	675
10	15.0	102.79	63.8	4.25	425

the fact that the particle distribution has a limited capacity for condensing vapor. When the changes of state are rapid,

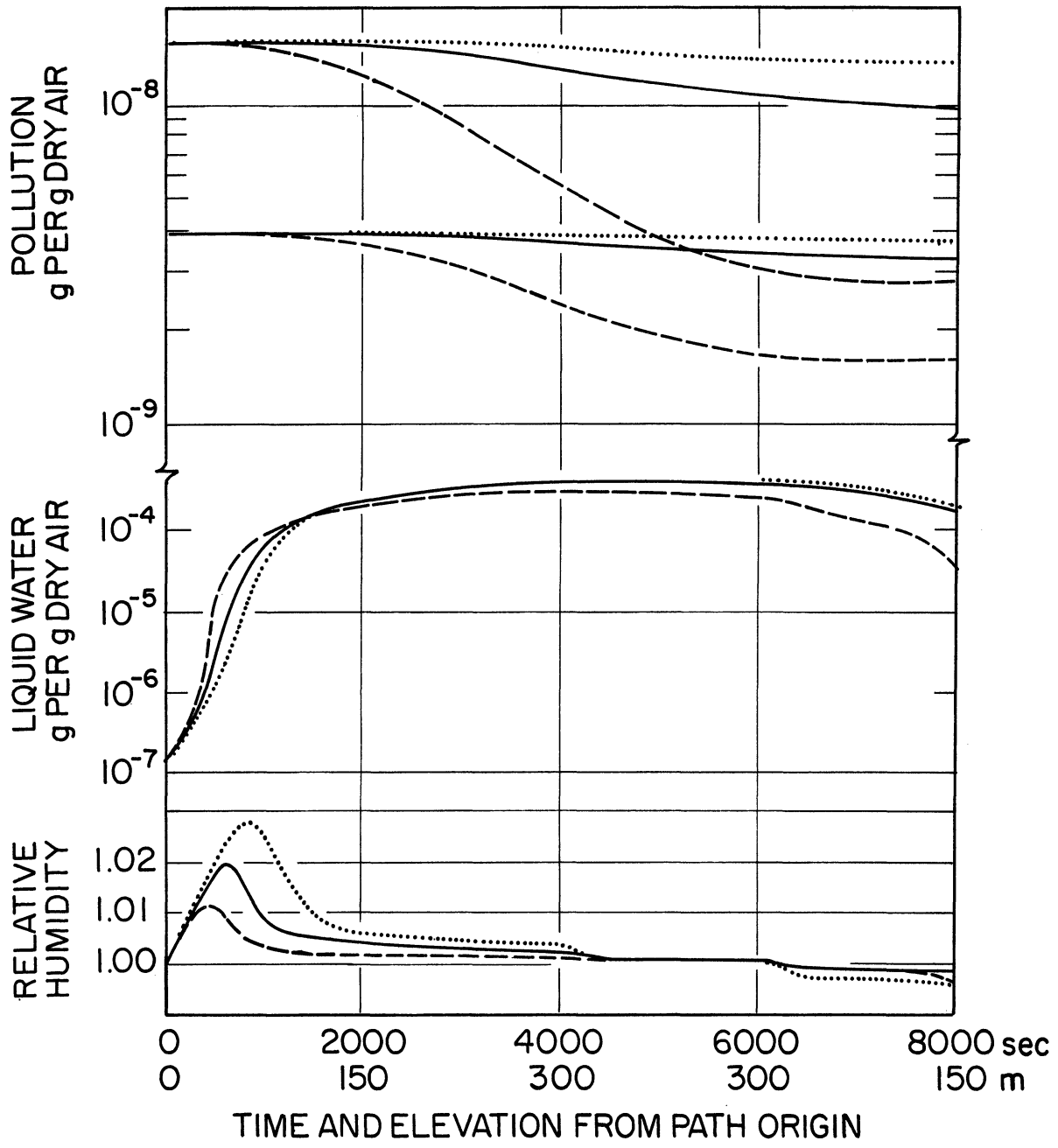

Figure 8.3 Course of relative humidity, liquid water and pollution amount along the path under wind speeds of 2 (broken line), 5 (solid), and 10 m sec^{-1} (dotted).

the vapor supply easily exceeds the condensation capability. The slower rates of change allow better correspondence between the vapor supply and the condensation rate. The early values of liquid water content also reflect this effect.

The strong contrast in the rates of removal of pollution between the low and high wind cases is an interesting feature. Two factors contribute to this effect: droplet size and duration of the rain-washing process. In the low-wind case, the droplets become larger (Fig. 8.4) and the rain field has five times longer to operate on the pollution cloud than in the high-wind case. The total effect is accentuated by a positive feed-back in that removal of drops from the cloud by scavenging enables the remaining drops to increase their growth rates which in turn increases their scavengeability more rapidly.

8.3 RAINFALL RATE

The immediate effect of increased rainfall is increased scavenging of pollution as well as water (Fig. 8.5). However, the removal is far from proportional with rainfall. Many factors probably work together to bring about such a result, some of which may be mentioned. A shift towards larger raindrops is associated with increased rainfall, and this normally leads to smaller efficiency per mass unit of water.

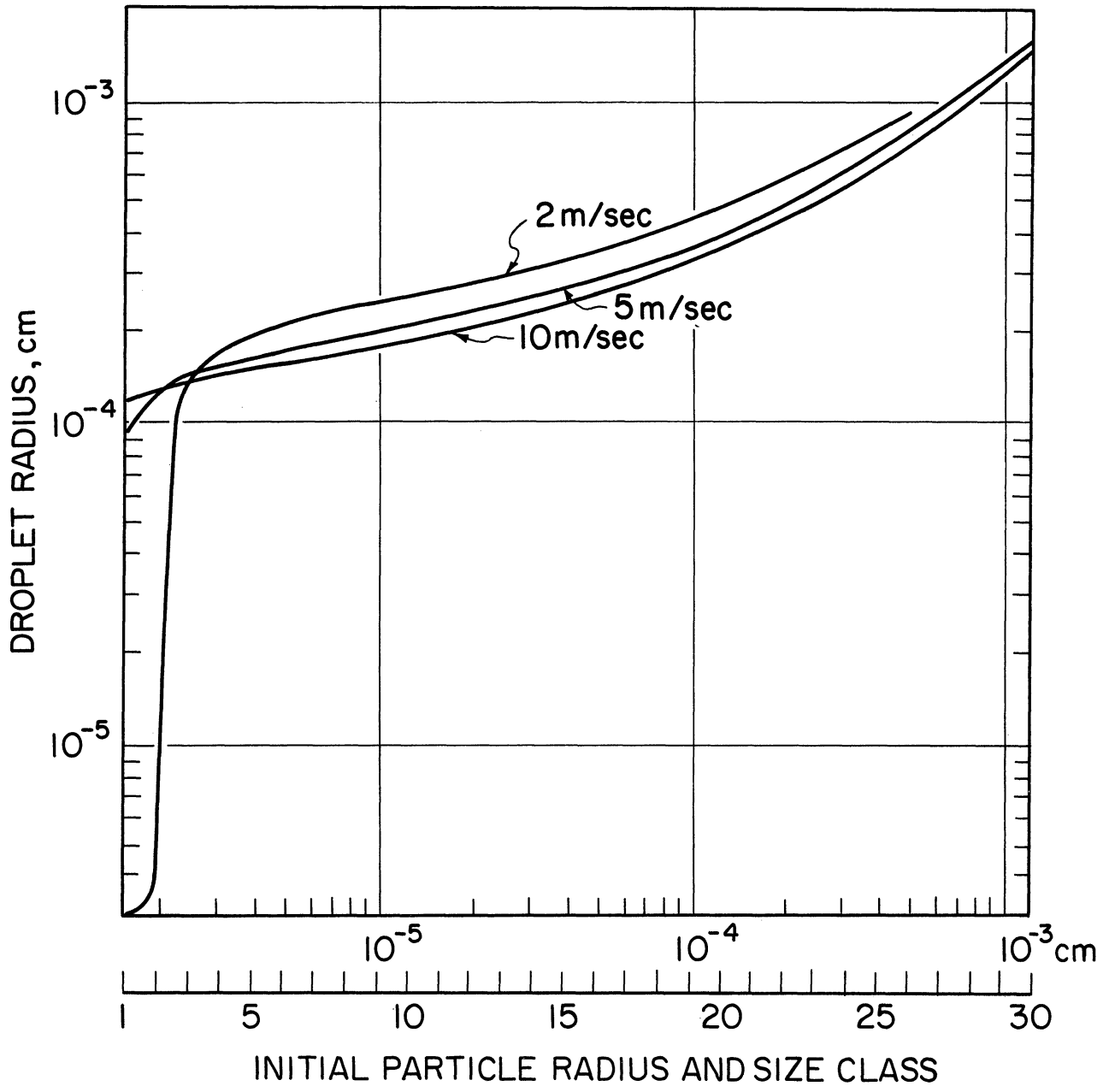

Figure 8.4 Droplet sizes at the top of the ascent for different wind speeds. Curves are labeled in m sec^{-1}.

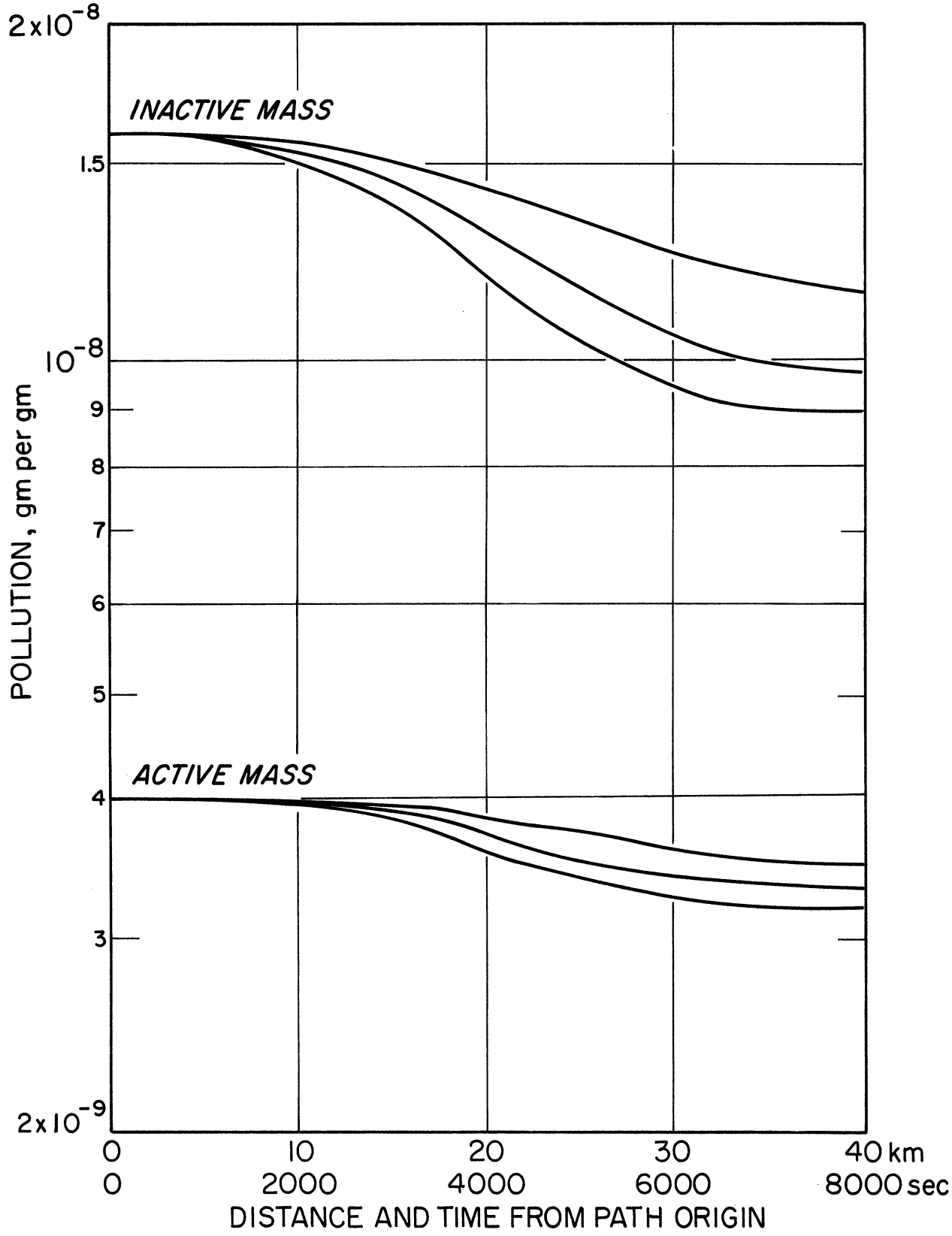

Figure 8.5 Pollution remaining in the air as a function of position along the path and rainfall intensity. Upper curves represent the inactive mass, lower curves the active mass; rainfall rates from top are 2, 5, and 10 mm hr^{-1}.

Figure 8.6 shows the number of particles left midway on the plateau. Those droplet sizes which are easily scavenged, are quite depleted even for the lowest rainfall rate shown. Early scavenging for high rainfalls is not enough to promote the next smaller size class into the effectively scavenged region within the time limit of the model (5,000 sec).

8.4 AIR TEMPERATURE AND HUMIDITY

Inasmuch as these variables represent the state of the air and the cloud and have an effect upon the air density, they affect also the several mixing ratios that express the concentrations of water vapor, liquid water, and pollution. In addition, increased temperature leads to increased vapor condensation per unit of cooling. Figure 8.7 shows how the droplet sizes change in response to the initial temperature. The size effect would be more pronounced if the number density of particles were constant. Reduced density of warmer air requires a larger pollution mixing ratio when the pollution is initially specified in terms of amount per unit of volume. Increased scavenging of both water and pollution (Fig. 8.8) again follows the increased drop sizes (hence increased temperature).

The relative humidity is a direct measure of water vapor amount when temperature is held constant. It is therefore obvious that (Fig. 8.9) the humidity peak should be attained later for the 90 per cent case than for the 100

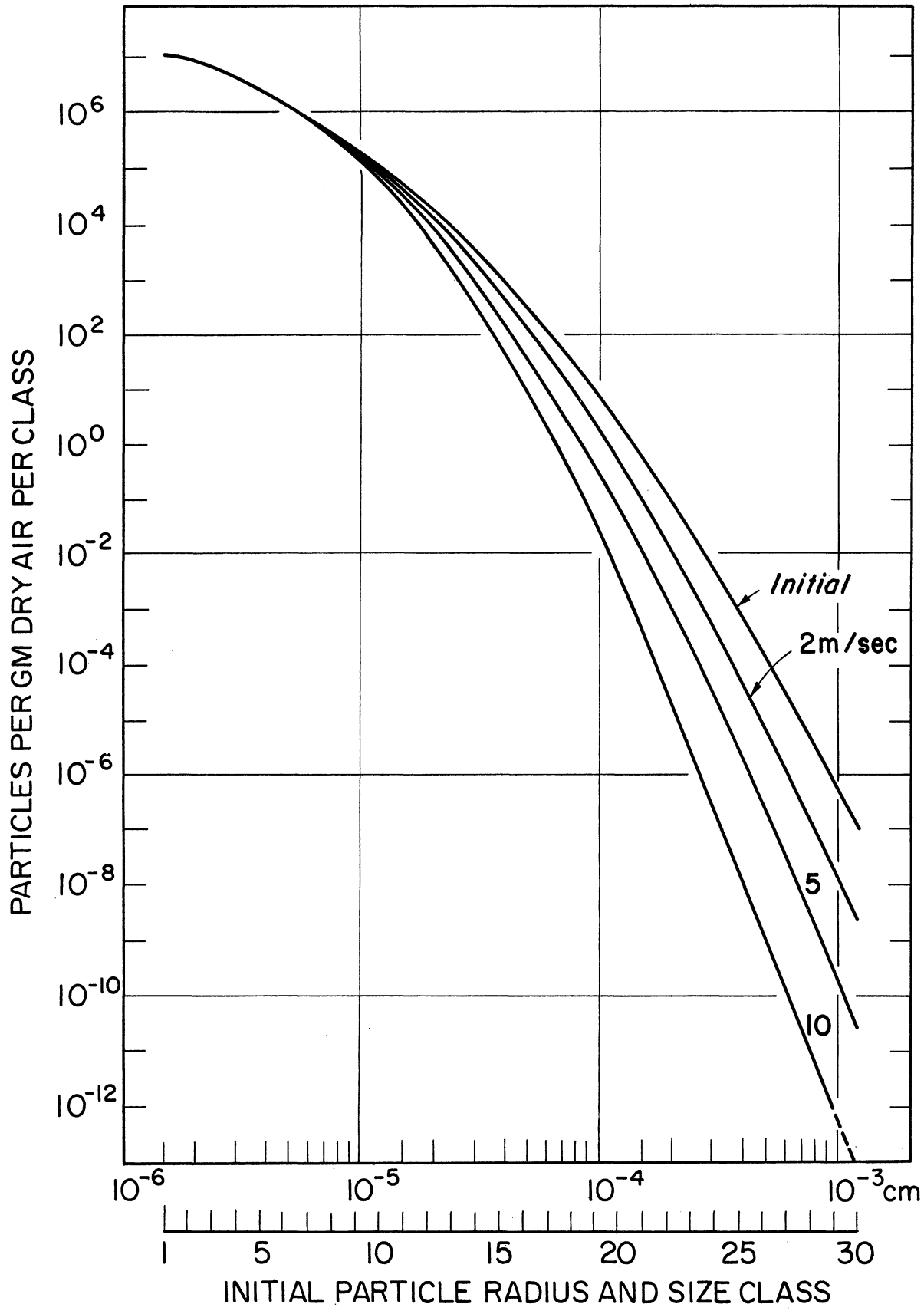

Figure 8.6 Number density of particles in each size class remaining in the air at the middle of the plateau, as a function of rainfall intensity.

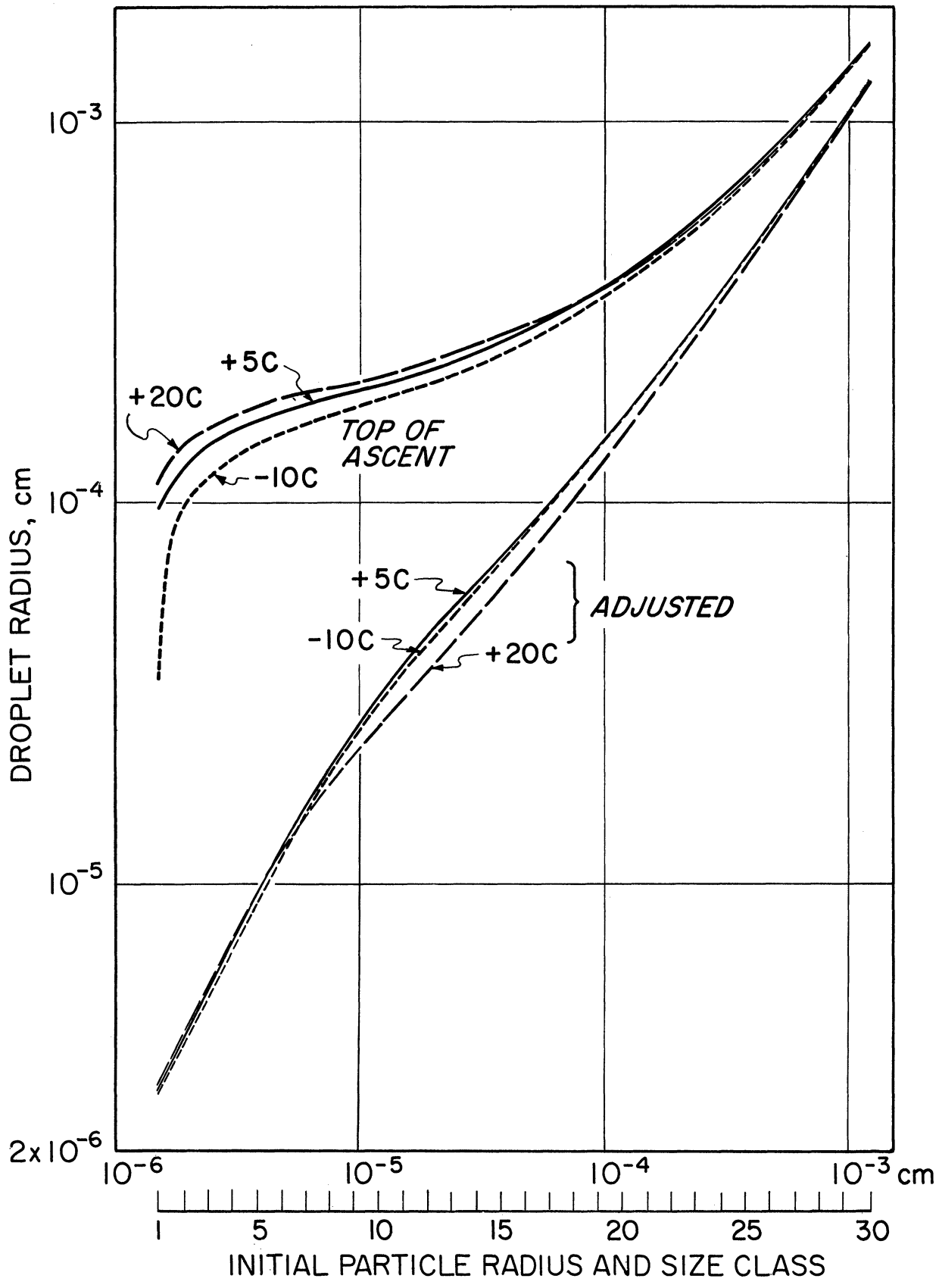

Figure 8.7 Droplet sizes for different initial air temperatures. Lower curves at origin (adjusted); upper curves at the top of the ascent.

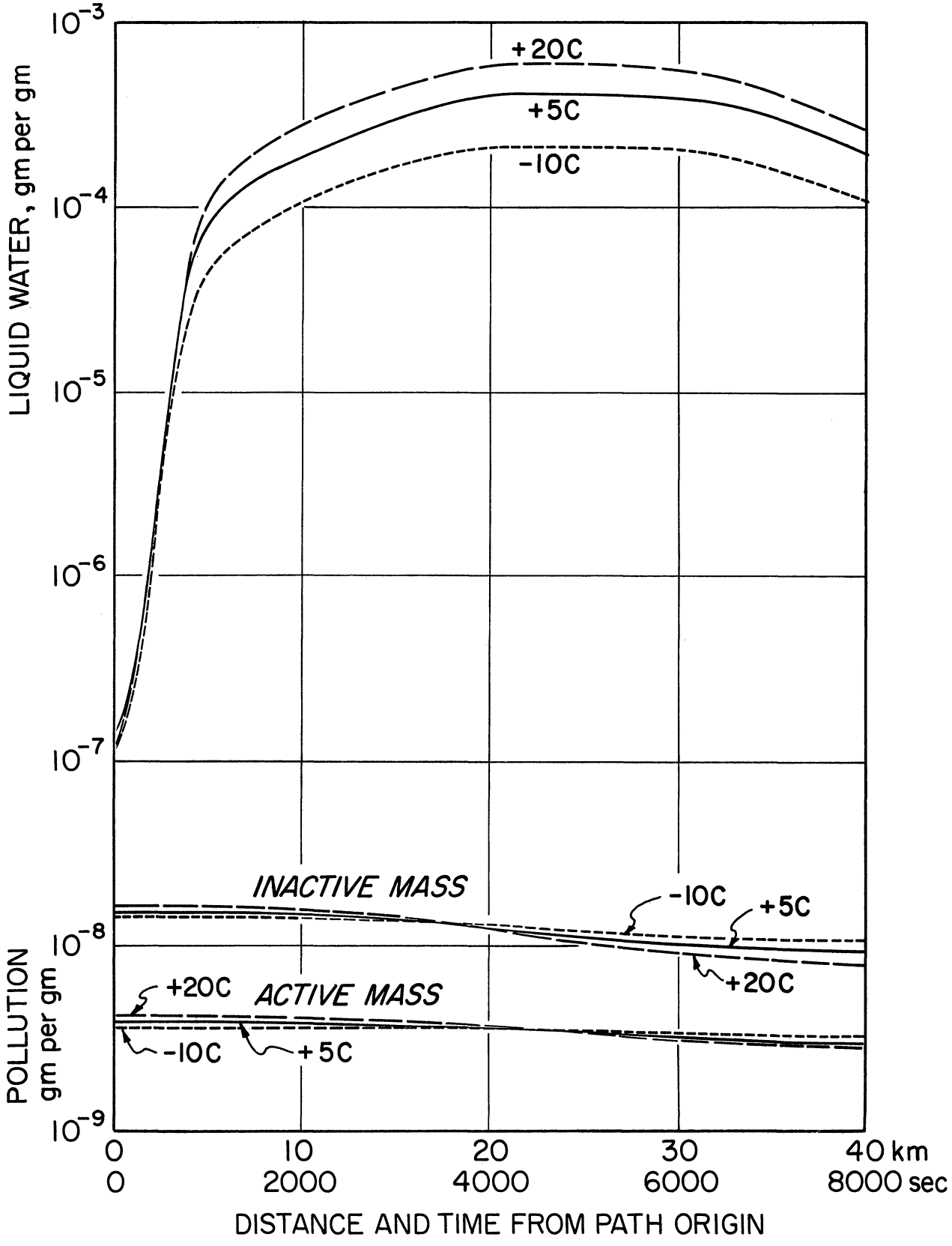

Figure 8.8 Course along the path of liquid water and pollution mixing ratios (gm per gm of dry air) for different initial air temperatures. Upper curves, liquid water; middle, inactive component; lower, active component.

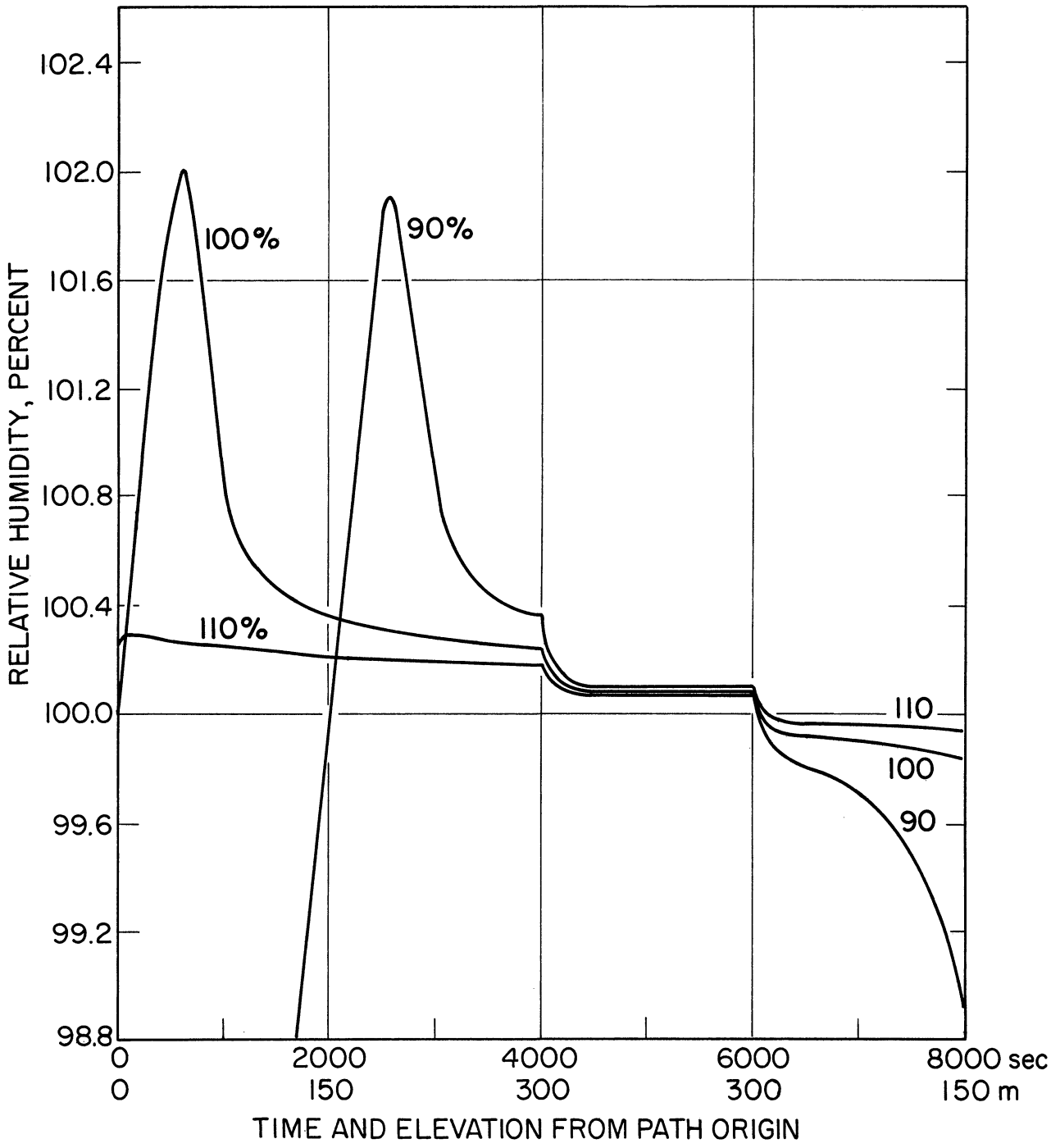

Figure 8.9 Course of relative humidity along the path for different initial humidities. Labels are initial relative humidity per cent values.

per cent case. In the 110 per cent case, this peak is passed during the preliminary adjustment period (Figure 8.10), so that when the path is entered, the droplets already present are capable of consuming the vapor as it becomes available. Again, the scavenging rate responds to the droplet size,so that increased scavenging follows increased humidity.

DISCUSSION AND CONCLUSION

The intent of the present study is to examine a situation of scavenging in a heavily polluted air flow through which rain falls from above. Within the limits of the model, scavenging depends on a number of parameters, temperature, humidity and pressure of the air, hygroscopicity, amount and size distribution of the pollution, and ascent and descent course of the air flow. Obviously only a fraction of possible variations in the different parameters has been examined, and further, the range examined does not necessarily cover the most interesting regions. However, indications of the type and magnitude of influence are apparent in the results.

The growth patterns shown by these computations differ in important respects from those found by Howell (1949), Mordy (1959), and Neiburger and Chien (1960). In each of the earlier studies the large nuclei appear to acquire all the available water and to deplete the supply so rapidly as to prevent growth upon the smallest nuclei. The demarcation

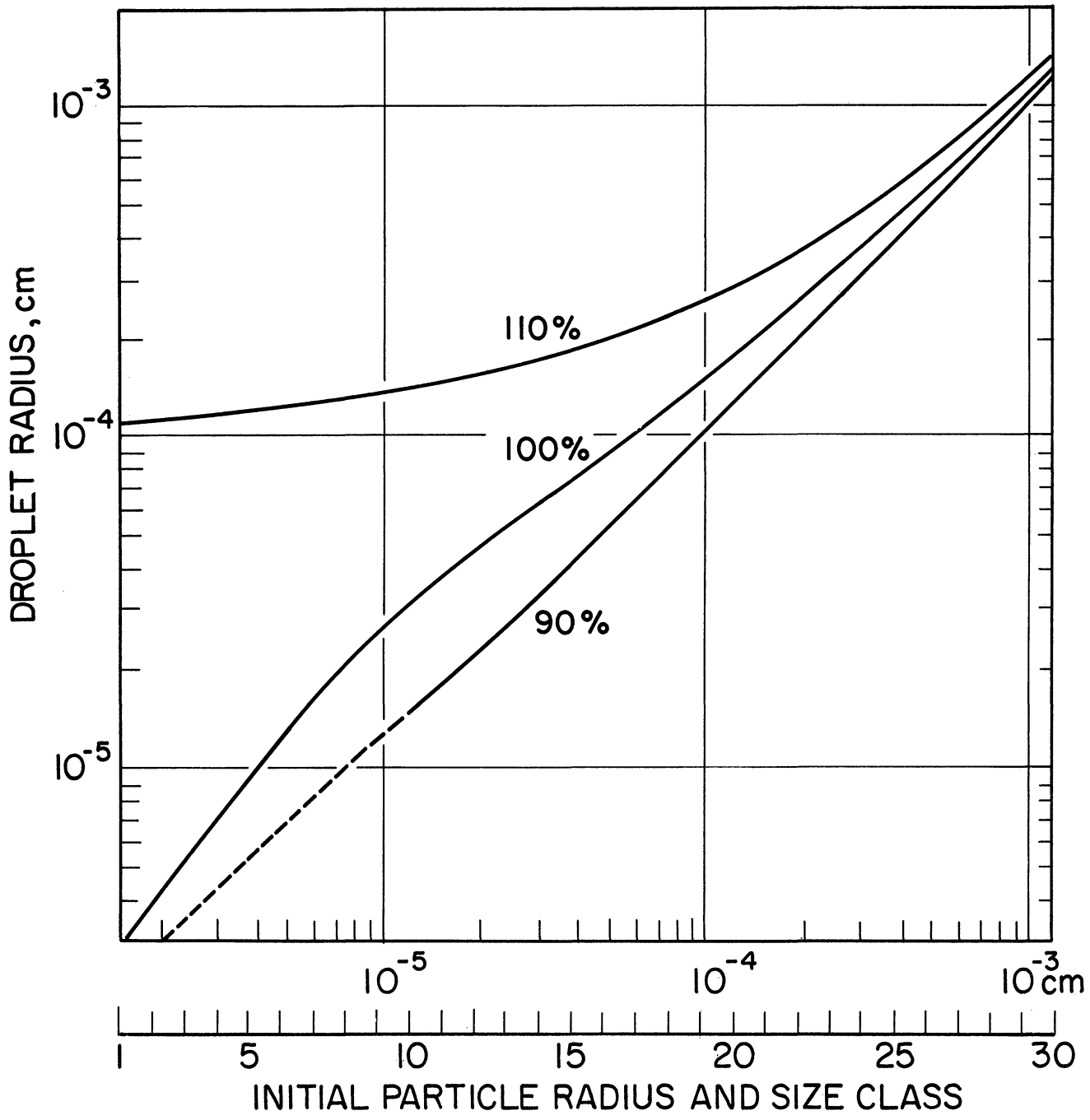

Figure 8.10 Droplet size spectra after preliminary adjustment for different initial humidities. Labels are initial relative humidity values in per cent.

point between growth and non-growth appears to be near 10^{-5} cm radius. Mordy's computations show it to occur as low as 3×10^{-6} cm and as high as 2×10^{-5} cm depending upon the initial nucleus spectrum and rate of rise. In no case do salt particles as small as 2×10^{-6} cm radius grow into cloud droplets according to Mordy's results. Neiburger and Chien's results are similar in this regard.

In contrast, the present computations indicate growth of all particles considered, ranging from 1.5×10^{-6} to 1.22×10^{-2} cm in radius (Fig. 7.3). This difference is primarily attributed to the thermal differences across the droplet size spectrum. Inasmuch as the large droplets are warmer than smaller ones, the equilibrium vapor densities over the droplet surfaces tend to hold back the growth rate of the larger droplets relative to the smaller ones.

The numerical method adopted for the present work specifically accounts for temperature and hygroscopicity of thirty size classes initially specified by the masses of the dry pollution particles. Also, in the present case, the particles are modeled as mixed nuclei composed of ammonium sulfate and graphite, as distinct from the pure sodium chloride nuclei assumed in the previous studies. Evaluation of the changes of droplet growth pattern attributable to the chemical differences remains to be done.

Another sharp difference from earlier results is the attainment of relative humidities in excess of 102 per cent.

This arises from the fact that the growing droplets are necessarily warmer than the air environment. In the baseline case the highest read-out relative humidity of 102.157 per cent is achieved after 600 sec of upward displacement at a rate of 7.5 cm sec^{-1}. The droplet temperatures range from 0.18 to 0.37 C above the air temperature, and the equilibrium relative humidities over the droplet surfaces (against saturation at air temperature) range from 101.994 to 102.114 per cent at this same time. Thus although it is true that the air supersaturation with respect to the droplet surfaces is very low (maximum of 100.160 per cent) in line with earlier results, the supersaturation with respect to the air temperature within the cloud is much higher than shown by the previous studies.

The peak of relative humidity is formed because the total condensation capability of the droplet assembly is limited in the early stages. This capability increases as the droplets grow. Prior to the humidity maximum the total droplet volume increases by a factor of some hundreds. No abrupt breaks in the size dependence of condensation capacity are shown. When enough drops of sufficient size are present (110 per cent relative humidity case, adjusted, Figure 8.10), the early stage humidity peak does not occur (Fig. 8.9).

The droplet size distribution is noticeably influenced by the super vapour pressure during condensation. High supersaturation produces a narrower size distribution than a lower one, but the distribution is always smooth and

droplet size increases with original particle size.

The concentration of particles is the overall important parameter influencing the average droplet size. This is an obvious statement when it is remembered that for reasonable concentrations relative humidity is seldom far from saturation, apart from the early peak, and the liquid water must be divided among the nuclei available.

Scavenging efficiency of droplets is closely linked to their size. In the model a sort of stepfunction is involved, since no capture by raindrops occurs for droplets smaller than 2 μm radius. This artificial barrier probably does not have much influence on the gross features of the study.

Because of the droplet size dependence, the proportional scavenging of pollution increases with increasing initial relative humidity and temperature and with decreasing particle number. Higher rainfall rate obviously increases the scavenging rate.

Scavenging of water shows similar features to that of pollution. The amount brought down is fairly low with the rather heavily polluted air examined. More pure country air or sea air should be apt to produce bigger droplets, with a resulting influence on rainfall pattern or mechanisms closer to that observed (Bergeron, 1960) or deduced from other measurements (Storebø, 1968).

The methods applied in this model, by avoiding the usual assumptions of elaborate theoretical derivations, preserve intact the small thermal differences among droplets in a growing haze-fog situation. Because all droplet growth takes place by virtue of the vapor gradients that depend strongly upon the droplet temperatures, the methods and the results provide new insights into the details of cloud formation.

In addition to the pollution and water-scavenging processes explored here, useful application of the method to studies of the development and removal of haze and fog in natural and polluted situations and to studies of rain production appears feasible. The introduction of suitable optical data into the system is also suggested as a means to model the changes of visibility and of the scattering and absorption of radiant energy under haze, fog and cloud conditions.

REFERENCES

Bergeron, T., 1960. Problems and methods of rainfall investigation. In Physics of Precipitation , Geophysical Monograph No. 5., Amer. Geophys. Union, Wash. D.C., pp. 5-30.

Byers, H.R., 1965. Elements of Cloud Physics, Univ. of Chicago Press, Chicago. 191 pp.

Fuchs, N.A., 1959. Evaporation and Droplet Growth in Gaseous Media. Pergamon Press, Oxford.

Goff, J.A. and S. Gratch, 1946. Low-pressure properties of water from -160 to 212 F. Trans. Amer. Soc. Heating and Ventil. Engineers, 52, 95-121.

Granat, L. , 1972. Deposition of sulfate and acid with precipitation over Northern Europe. Rep. No. AC-20, Inst. of Meteorology, Univ. of Stockholm.

Harned, H. L., and B. B. Owen, 1958. Physical Chemistry of Electrolytic Solutions, 3rd. ed. Reinhold Pub. Co., New York. 803 pp.

Hodgman, C. D., 1961. Handbook of Chemistry and Physics. 43rd ed. Cleveland, Chem. Rubber Pub. Co.

Howell, W.E., 1949. The growth of cloud drops in uniformly cooled air. J. Meteor., 6, 134-149.

Langmuir, I., 1944. Super cooled droplets in rising of cold saturated air. General Electric Company, Schenectady, N.Y., 150 pp.

Low, R.D.H., 1969a. A generalized equation for the solution effect in droplet growth. J.Atmos. Sci., 26, 608-611.

Low, R.D.H., 1969b. A theoretical study of nineteen condensation nuclei. J. Recherches Atmosphériques, 4, 1re année, 65-78.

Maxwell, J., 1927. Theory of the wet-bulb thermometer. Scientific Papers, Volume 11.

Mordy, W.A., 1959. Computations of the growth by condensation of a population of cloud droplets. Tellus, 11, 16-44.

Neiburger, M., and C.W. Chien, 1960. Computations of the growth of cloud drops by condensation using an electronic digital computer. In Physics of Precipitation, Geophys. Monograph No. 5, Amer.Geophys. Union, Wash. D.C., pp. 191-210.

Rooth, C., 1957. On a special aspect of the condensation process and its importance in the treatment of cloud particle growth. Tellus, 9, 372-377.

Squires, P., 1952. The growth of cloud drops by condensation. I. General characteristics. Australian J. Sci. Res., A. 5, 59-86.